PERIODICO di MINERALOGIA
established in 1930

DIPARTIMENTO
DI SCIENZE DELLA TERRA

SAPIENZA
UNIVERSITÀ DI ROMA

An International Journal of
Mineralogy, Crystallography, Geochemistry,
Ore Deposits, Petrology, Volcanology
and applied topics on Environment, Archaeometry and Cultural Heritage

Fluid inclusion studies on Cu-Mo-Au bearing quartz-sulphide veins and veinlets in Qarachilar area, Qaradagh pluton (NW Iran)

Vartan Simmonds[*,a] and Mohssen Moazzen[b]

[a] Research Institute for Fundamental Sciences, University of Tabriz, 29 Bahman Blv., 51666 Tabriz, IRAN

[b] Geosciences Department, University of Tabriz, 29 Bahman Blv., 51666 Tabiz, IRAN

ARTICLE INFO

Submitted: February 2016
Accepted: October 2016
Available on line: October 2016

* Corresponding author:
simmonds_vartan@tabrizu.ac.ir

DOI: 10.2451/2016PM658

How to cite this article:
Simmonds V. and Moazzen M. (2016)
Period. Mineral. 85, 261-276

ABSTRACT

The Qaradagh pluton is located in NW Iran. It is comprised of Eocene-Oligocene intrusive pulses and hosts hydrothermal alterations and vein-type Cu-Mo-Au mineralization, which is more manifested at Qarachilar area (central part of the Qaradagh pluton). This study aims to elucidate the physico-chemical characteristics of the ore-bearing fluid using microthermometric studies on quartz-sulphide veins/veinlets. Microthermometric analyses show that the salinity of ore-bearing fluid is about 15-65 wt% $NaCl_{equiv}$, with the highest frequency between 25 and 45 wt% $NaCl_{equiv}$. The homogenization temperature for primary 2-phase and multiphase inclusions is about 220-540 °C. Most of the 2-phase inclusions homogenize by vapor disappearance with $T_{H(L-V)}$ values between 280 and 440°C. Most of the analyzed multiphase inclusions homogenize by simultaneous disappearance of vapor bubble and dissolution of halite daughter crystal, for which the T_H value is 240-420 °C. The data-points trend in $T_{H(L-V)}$-Salinity plot indicates the occurrence of boiling of low-salinity fluids and dilution by superficial fluids. The minimum pressure at the time of fluid entrapment is estimated about 50 to 120 bars, equivalent to the hydrostatic depths of 500 to 1100 m.

Keywords: Qarachilar; Qaradagh pluton; Fluid inclusion; Microthermometry; Salinity; Homogenization temperature.

INTRODUCTION

Subduction of the Neo-Tethyan oceanic crust beneath the central Iranian domain occurred during the Alpine orogeny in the late Mesozoic and early Cenozoic (Berberian and King, 1981; Alavi, 1991) and led to the formation of the Urumieh-Dokhtar magmatic arc (UDMA). The UDMA extends from northwest to southeast of Iran over nearly 2000 km, which correlates with the nation's porphyry copper metallogenic belt, comprised of several metallogenic zones, and hosts most of the major and small porphyry copper deposits (PCDs) and prospects in Iran, including the Sarcheshmeh (central Iran; Shahabpour, 1982) and Sungun PCDs (NW Iran, neighboring the Qaradagh pluton; Calagari, 1997, 2004a; Hezarkhani and William-Jones, 1998).

The Qaradagh pluton, located at the northernmost part of the UDMA (46°20'E to 46°24'E lat. and 38°49'N to 38°53'N long.) (Figure 1), intruded the upper Cretaceous and Paleocene flysch-type sedimentary, volcanoclastic and volcanic (submarine basic to intermediate in nature), as well as Eocene volcanic (mainly andesitic) rocks at several discrete pulses during the middle Eocene-Oligocene (e.g., Amini Fazl, 1994; Mokhtari, 2008; Simmonds and Moazzen, 2015). According to Mokhtari

et al. (2005) the Qaradagh pluton is comprised of mafic to felsic rock types including gabbro, diorite, quartz diorite, quartz monzonite, quartz monzodiorite, leucotonalite, granodiorite, monzogranite and sub-volcanic porphyritic granite. These rocks belong to I-type and calc-alkaline active continental margin granitoids (Mokhtari, 2008), showing geochemical characteristics of subduction related volcanic arcs (Zakeri, 2013).

The magmatic-hydrothermal fluids derived from this intrusive complex produced hydrothermal alterations within and around the pluton and stock-work and vein-type Cu-Mo-Au mineralization. The most pronounced occurrences are in Qarachilar, Qaradareh, Zarlidareh, Anigh and Pirbolagh (Figures 1 and 2).

This study focuses on the physico-chemical characteristics of the ore-bearing fluid responsible for Cu-Mo-Au mineralization in the Qarachilar area, central part of the Qaradagh pluton, and the main factors involved in

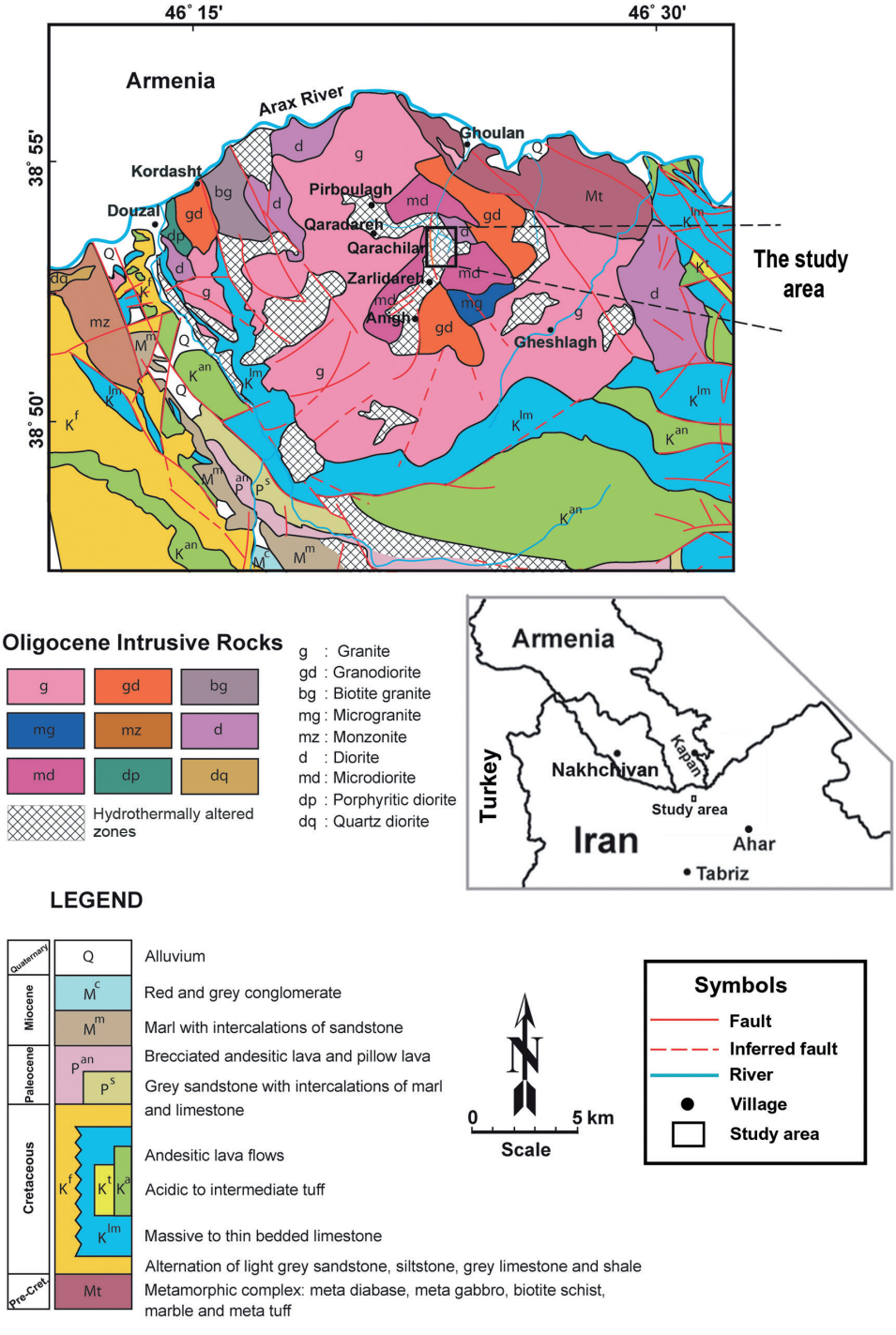

Figure 1. Geologic map of the Qaradagh pluton and the study area (simplified and modified after Mehrpartou et al., 1997).

ore precipitation using microthermometric studies on fluid inclusions trapped within the quartz-sulphide veins and veinlets.

BACKGROUND INFORMATION ABOUT THE STUDY AREA

Petrography of the granodioritic host rock

The dominant lithology in the Qarachilar area is granodiorite, which hosts the quartz-sulphide veins and veinlets (Figure 2). It is composed of plagioclase (fresh, euhedral to subhedral; 40-60%), K-feldspar (orthoclase, medium to fine-grained, anhedral with perthitic, granophyric and monzonitic textures; 5-15%) and quartz (anhedral, medium to fine grained with mosaic and intergranular textures; 15-25%), with subordinate amounts of biotite (fresh, booklet-shape and subhedral; 5-15%), amphibole (euhedral to subhedral; 0-10%), pyroxene (scarce and subhedral; 0-5%) and opaque minerals (euhedral to anhedral; 0-5%), displaying hetero-granular and monzonitic textures (Figure 3 a,b). Accessory minerals are apatite, zircon and titanite.

Hydrothermal alteration

The magmatic-hydrothermal fluids originated from the intrusive phases have produced various hydrothermal alteration zones across the pluton, including potassic, phyllic/sericitic, argillic and propylitic alterations and silicification. The main alteration zones developed in the Qarachilar area are potassic and phyllic/sericitic, which encompass the Cu+Mo+Au±Ag mineralization and which become more profound where fractures are present. Moreover, envelopes of mainly sericitic/phyllic alteration surround the quartz-sulphide veins and veinlets.

The potassic alteration zone is characterized by the formation of fine flakes of secondary biotite (reaching

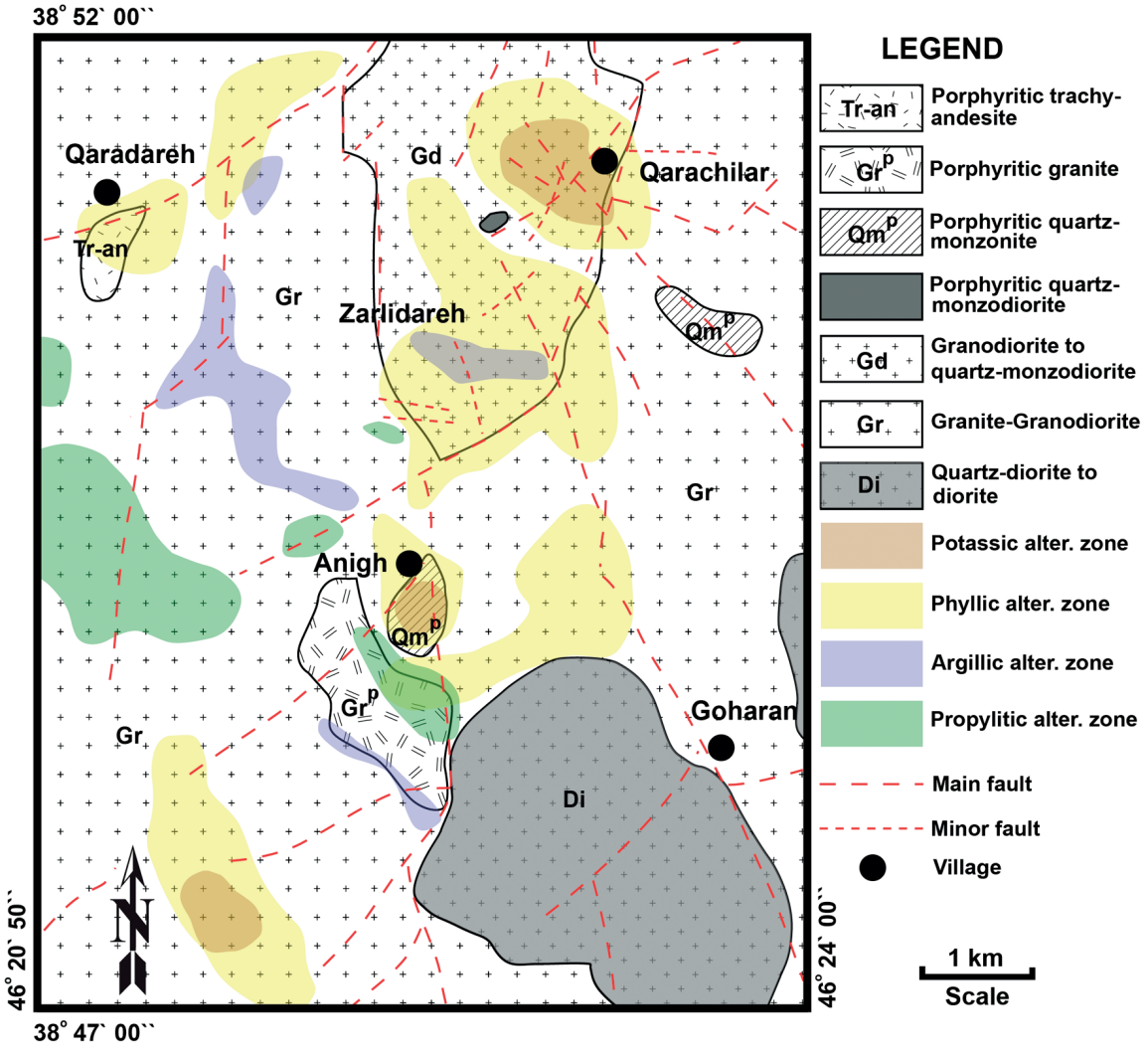

Figure 2. Simplified geologic and alteration map of the Qarachilar area (after Zakeri, 2013).

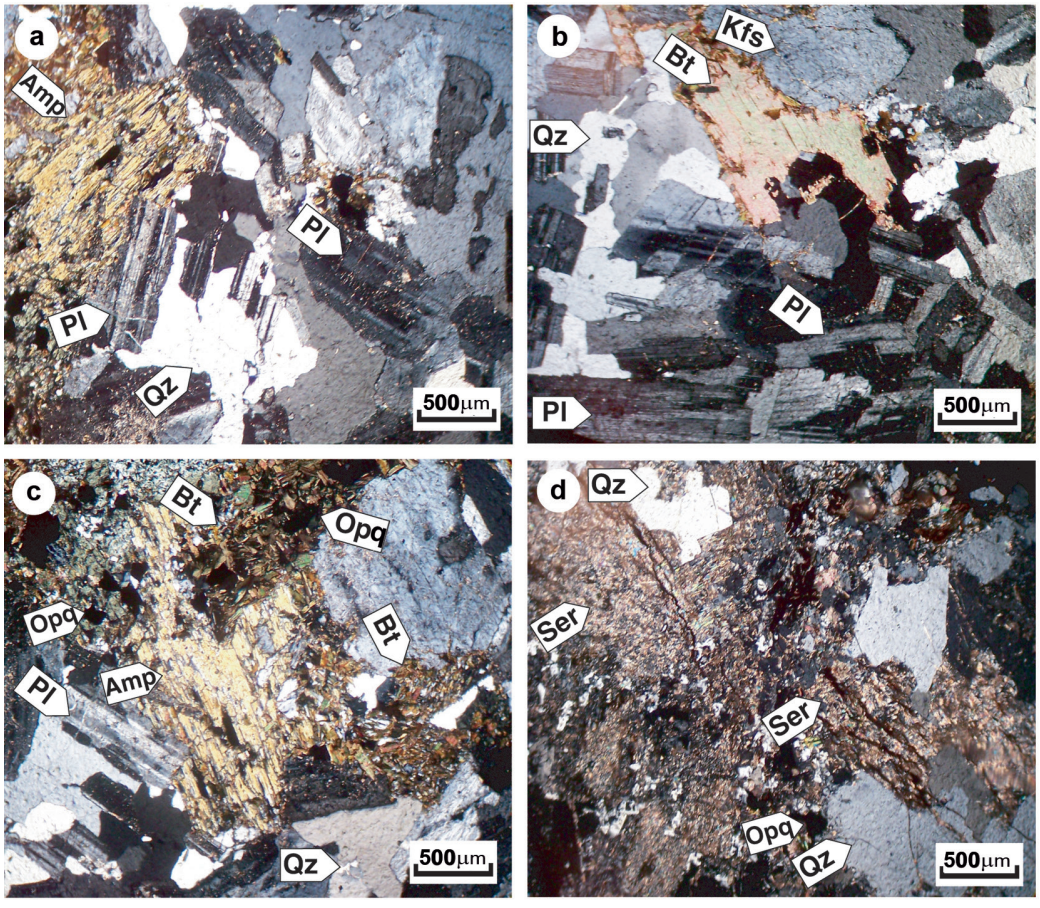

Figure 3. Microphotographs of the granodioritic host rock and its alteration. (a) and (b) Granular texture comprised of plagioclase with poly-synthetic twining, subhedral amphibole and anhedral quartz and biotite; (c) potassic alteration characterized by the formation of tiny flakes of neo-formed biotite replacing the primary biotite and amphibole or occurring as disseminations within the background; (d) phyllic alteration recognizable by the moderate to intense sericitization of feldspars and the formation of opaque minerals. Mineral name abbreviations from Whitney and Evans (2010).

up to 20%) and fine-grained anhedral and intergranular orthoclase (8-10%), along with opaque minerals (magnetite, chalcopyrite and pyrite) (Figure 3c).

Phyllic alteration zone is marked by sericitization of feldspars and replacement of ferro-magnesian minerals by sericite and chlorite, accompanied by the formation of secondary quartz and pyrite (Figure 3d). The sericite content reaches 40-70%.

Hypogene and supergene mineralization

Hypogene mineralization in the Qarachilar area has occurred as quartz-sulphide and sulphide veins and veinlets, as well as disseminations of sulphides within the host rock. The quartz-sulphide and monomineralic sulphide veins-veinlets occur as parallel swarms, comprised of two main veins and numerous veinlets and microveinlets (sheeted veins), as well as stock-work type cross-cutting veinlets and have variable thicknesses, ranging from mm up to <1 m (Figure 4), mainly with NW-SE trends and 50-700 m length. The major sulphide minerals are pyrite, chalcopyrite and molybdenite, with lesser amounts of bornite and digenite (Figure 5). Pyrite (1-10%) is the most abundant sulphide mineral, while chalcopyrite (1-8%) is the main hypogene Cu sulphide (Figure 5 a,b). Molybdenite (up to -5%) occurs as large flakes or aggregates of anhedral, tiny shredded crystals, rosettes or plates with variable sizes of 200 μm to 3mm, disseminated within the quartz veins-veinlets, silicified zones and the host rock (Figure 5c).

Afterwards, supergene processes have affected the hypogene sulphides, leading to the development of a leached-oxidized zone, characterized by the intense leaching of primary sulphides and the formation of Fe oxides-hydroxides (limonite-goethite), ferrimolybdenite (yellow-colour tinges, probably along with powellite), malachite and azurite, and a sulphide-enriched zone beneath the paleo-water table, represented by the replacement of primary sulphides by covellite and chalcocite.

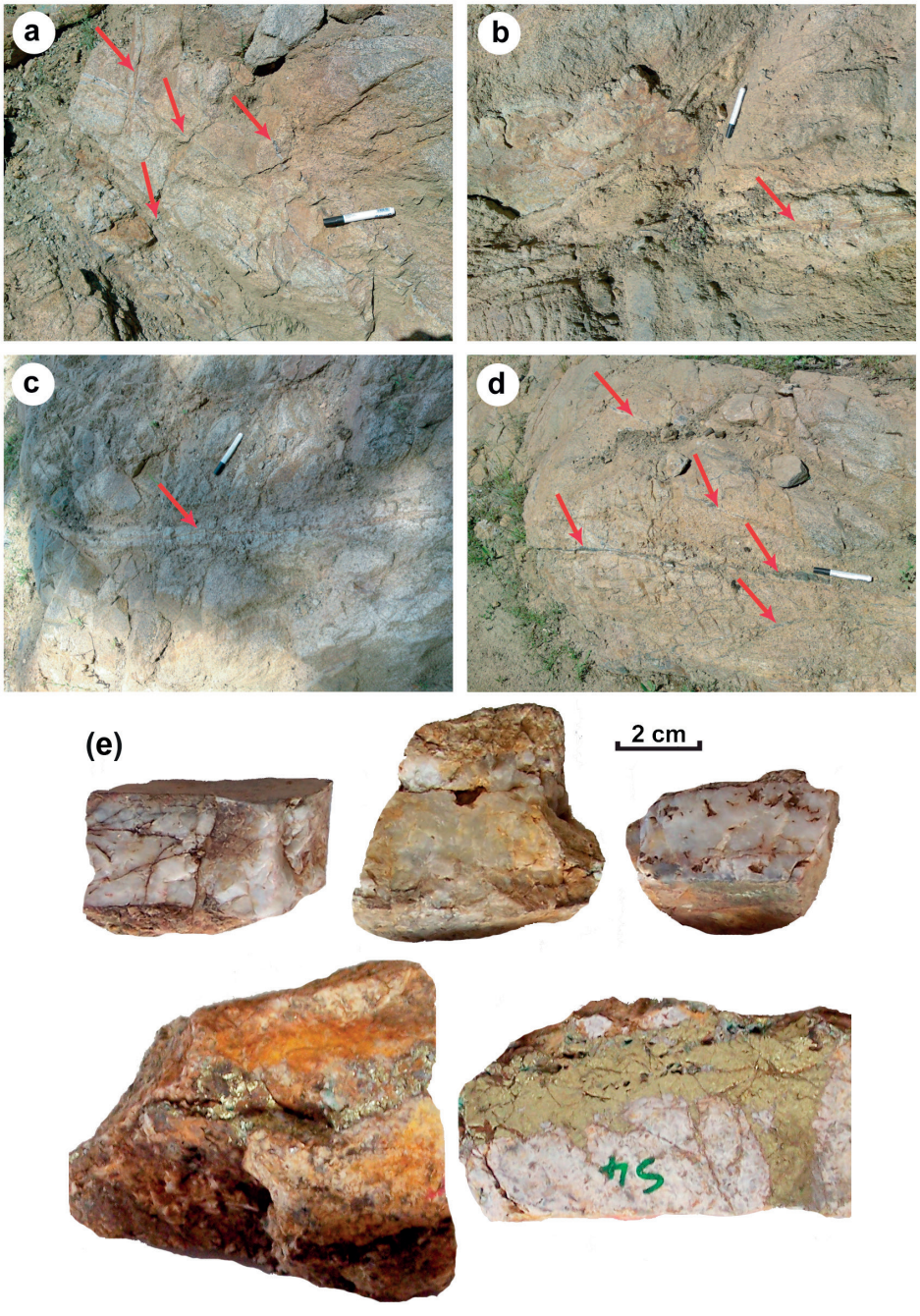

Figure 4. (a)-(d) Outcrops and (e) hand specimens of quartz-sulphide and monomineralic sulphide veinlets (shown by red arrows) within the granodioritic host rock, south of the Qarachilar village.

MATERIALS AND METHODS

Following field studies and sampling of the sulphide-bearing quartz veins-veinlets, as well as the host rock and hydrothermal alteration zones, petrographic and mineralogical studies were carried out at the Research Institute for Fundamental Sciences (RIFS), University of Tabriz. Fluid inclusion studies were mainly performed on the milky quartz-sulphide veins-veinlets containing chalcopyrite and molybdenite. For this, 10 samples were selected and doubly polished sections (~150 μm thick) were prepared and studied under the microscope. After microscopic examination, the wafers of 6 samples were

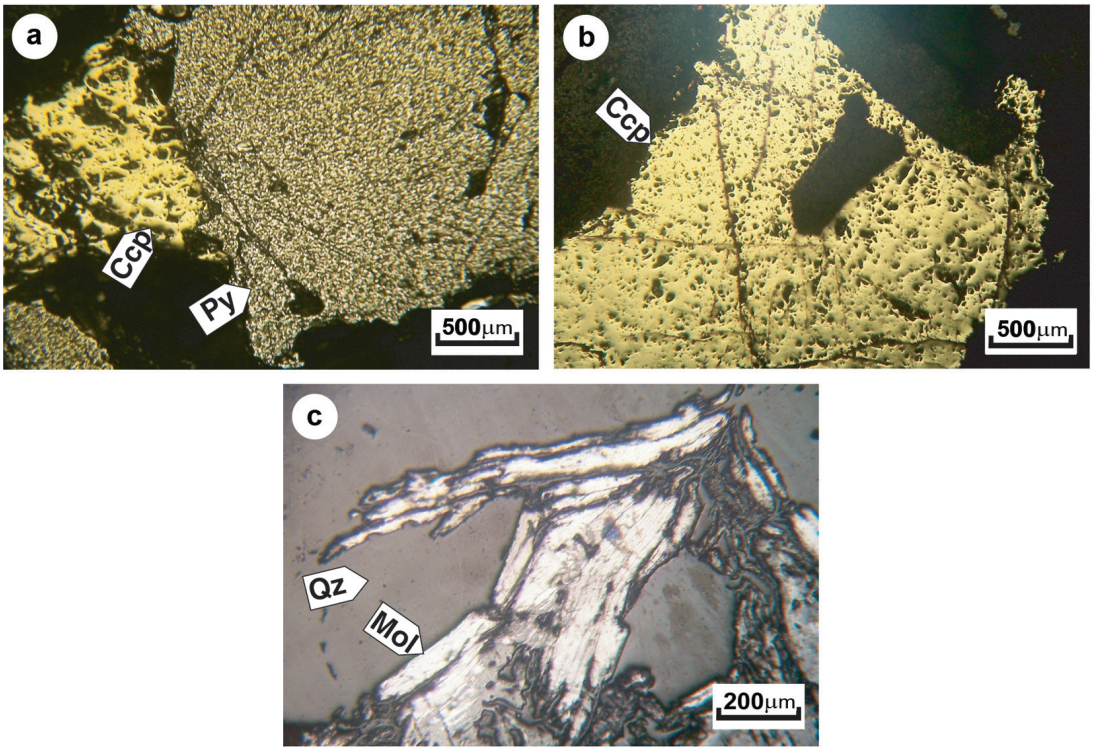

Figure 5. Microphotographs illustrating sulphide mineralization within the quartz-sulphide veins/veinlets. (a) Co-existence of pyrite and chalcopyrite within the quartz veins; (b) disseminations of chalcopyrite within the quartz veins and the host rock; (c) molybdenite flakes within the quartz veins, especially at their margins. Mineral name abbreviations from Whitney and Evans (2010).

subjected to microthermometric analysis, using a calibrated and standardized THMS600 Linkam heating-freezing stage, equipped with two heating (TP94) and freezing (LNP) controllers, attached to an Olympus petrographic microscope and a monitoring video apparatus. The precision of temperature measurements were estimated about ±0.5 °C for the range between -100 to 20 °C and ±5.0°C for the range between 100 and 450 °C.

Microthermometric analyses were carried out at the Mineralographic Laboratory of Payam Noor University, Tabriz, Iran. The bulk salinity of the fluid was calculated based on $T_{m(ice)}$ (Bodnar, 1993) or $T_{m(NaCl)}$ (Sterner et al., 1988). The density calculations for the studied inclusions were carried out according to Zhang and Frantz (1987).

RESULTS

Fluid inclusion petrography

The prepared doubly-polished sections of the sulphide-bearing quartz veins were examined under microscope in order to determine the distribution pattern, shape, size, phase content and paragenetic characteristics of the fluid inclusions and the daughter crystals. In the result, it was revealed that quartz crystals within these veins and veinlets are fluid inclusion-rich, containing randomly distributed relatively large-sized primary inclusions (up to 20 μm in size), as well as numerous trails of secondary fluid inclusions (≤5 μm), which sometimes cross-cut each other (Figure 6 a,b).

The observed primary inclusions mainly illustrate negative crystal, ellipsoidal, rounded, elongated and irregular shapes, in order of abundance (Figure 6). Necking-down is evident in some inclusions. The visible intergrowth between disseminated sulphides and quartz crystals testifies that they are cogenetic and precipitated from a common ore-bearing fluid. Therefore, the obtained data can be generalized to the ore formation conditions.

The primary inclusions are recognizable by their random distribution, relatively large size and relatively similar phase ratios (80% in most cases) (e.g., Hedenquist et al., 1998; Bodnar, 2003; Goldstein, 2003; Wanhainen et al., 2003; Seedorff and Einaudi, 2004; Bouzari and Clark, 2006) with no trails of secondary inclusions encompassing them. Secondary inclusions are identified by their distribution as trails cross-cutting the grain boundaries. Some of these trails are confined within the host crystals and can be considered as pseudo-secondary inclusions. Based on the classification of Kranz (1983) and Vollbrecht (1989), secondary fluid inclusions in the

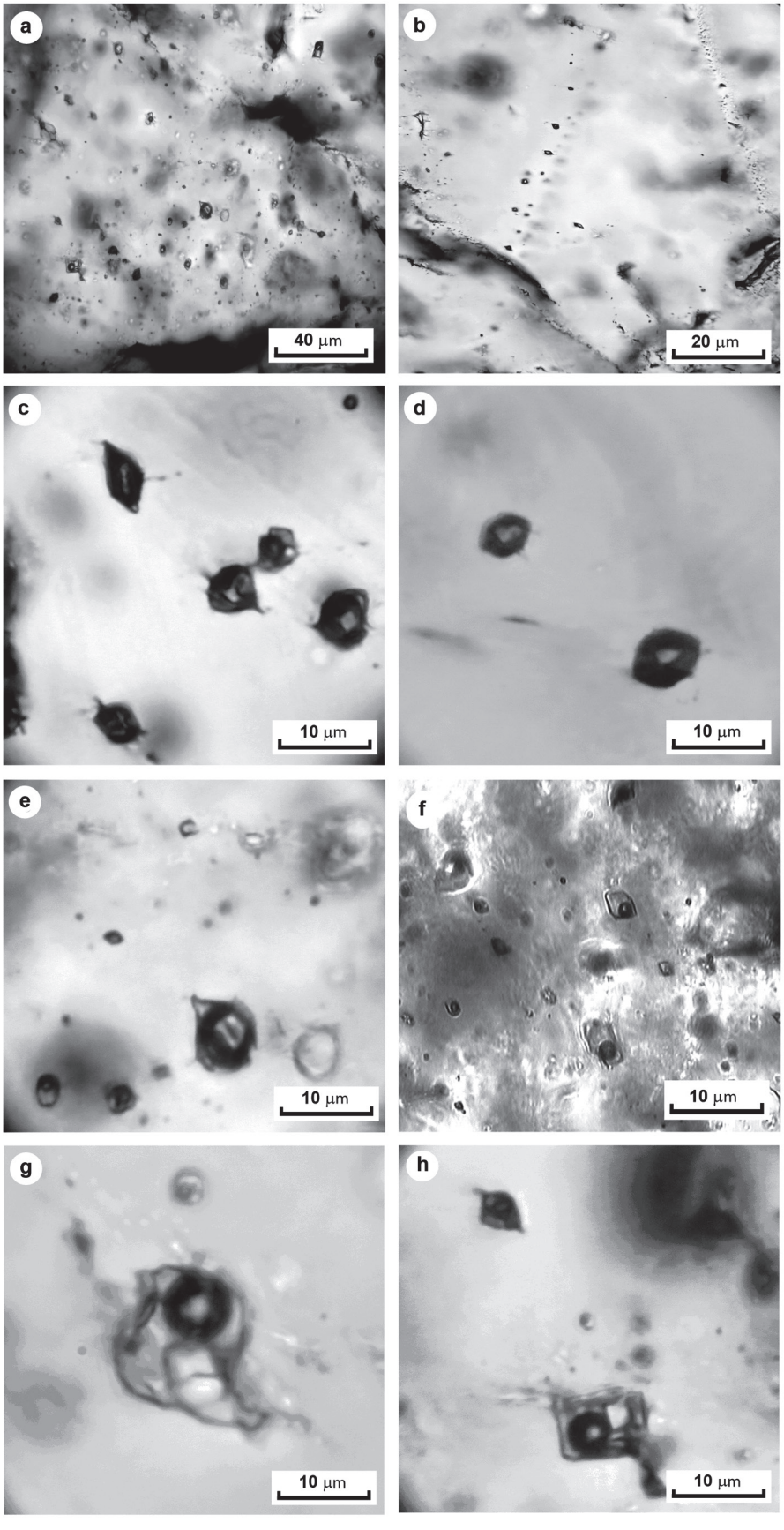

Figure 6. Microphotographs of fluid inclusions within the quartz-sulphide veins-veinlets. (a) 2-phase and multiphase inclusions within the quartz-sulphide veins; (b) trails of secondary monophase vapor and 2-phase fluid inclusions; (c) mono-phase vapor (type 1) and vapor-rich 2-phase (type 3) inclusions; (d) mono-phase vapor (type 1) inclusions with negative crystal shapes; (e) a 2-phase vapor-rich (type 3) inclusion; (f) 2-phase liquid-rich (type 2) inclusions; (g) a multiphase (type 4) inclusion containing halite and sylvite daughter crystals; (h) a multiphase (type 4) inclusion containing a halite daughter crystal.

studied samples appear as transgranular and transphase trails, while the pseudo-secondary inclusions are mainly intragranular (boundary to boundary, boundary to grain interior, and grain interior). As a whole, secondary inclusions are the most abundant type of fluid inclusions within the studied quartz samples.

Based on the phase content at room temperature, the studied inclusions are mainly categorized into four types, (1) Mono-phase vapor, (2) 2-phase liquid-rich (aqueous), (3) 2-phase vapor-rich, and (4) multiphase, containing a vapor bubble, an aqueous liquid and one or more solids (Figure 6). Additionally, very few small CO_2-bearing vapor-rich inclusions were also observed with a thin rim of CO_2 phase around the vapor bubble, which were not suitable for microthermometric analysis due to their small size and low degree of filling. Besides, microthermometric studies were performed on the primary and relatively large 2-phase (type 2 and 3) and multiphase (type 4) inclusions, which range in size from 2 to 10 μm and 4 to 20, respectively (Figure 6).

Multiphase (L+V+S) inclusions are relatively abundant, compared to 2-phase inclusions. They mainly contain halite and sylvite daughter minerals (Figure 6g,h), sometimes accompanied by tiny opaque crystals (dark-colour, most likely Fe oxides). In general, inclusions with halite daughter crystal are much common than those containing two or three solids.

The presence of halite daughter crystals indicates the NaCl-saturated state of the ore-bearing fluid, while sylvite crystals signify the saturation of KCl within it. It must be noted that some of the halite daughter crystals may have been entrapped as solid phases from the ore-forming fluid, especially where their size is too large compared to the host inclusion.

The approximately estimated degree of filling (the volumetric proportion of liquid phase to the total volume of the inclusion; Shepherd et al., 1985) for type 2 and 3 inclusions is about 70-80% and 20-30%, respectively, while it ranges from 10 to 30% for type 4 inclusions.

Microthermometric results

Homogenization temperature

Heating runs were performed on type 2, 3 and 4 inclusions. Coexistence of these types of inclusions and the type 1 (mono-phase vapor) inclusions can testify to their entrapment from a heterogeneous boiling fluid.

Most of the 2-phase inclusions (type 2) showed homogenization into liquid state by disappearance of vapor bubble, and their measured $T_{H(L-V)}$ values range from 280 to 440 °C with peak abundances between 300 to 360 °C and 380 to 420 °C (Figure 7a). Some 2-phase inclusions homogenized to vapor phase (type 3). Their $T_{H(L-V)}$ values lie within the range of 440-540 °C. Comparing the T_H values of these two types of inclusions shows that type 3 inclusions are homogenized at higher temperatures compared to type 2 ones.

Type 4 (multiphase) inclusions show three modes of homogenization. A large number of them are homogenized by almost simultaneous disappearance of halite crystal and vapor bubble, with T_H values between 240 and 420 °C and the peak abundance of measured values falling between 260 and 340 °C (Figure 7b). Those multiphase inclusions which homogenize by the dissolution of halite crystal show sparse homogenization temperatures ($T_{m(NaCl)}$), mainly ranging from 220 to 360 °C, along with few measurements within narrow ranges of 400-420°C and 520-540 °C (Figure 7c). A few multiphase inclusions are homogenized by disappearance of vapor bubble, with $T_{H(L-V)}$ values between 300 and 360 °C and a single measurement about 520-540 °C (Figure 7d). The dissolution temperature of sylvite daughter crystals within multiphase halite-sylvite-bearing inclusions varies between 87° and 161 °C with an average value of 141 °C.

Salinity determination

The salinity of 2-phase fluid inclusions (types 2 and 3) was measured by freezing procedure, while salinities of multiphase inclusions (type 4) were calculated using the melting temperature of halite daughter crystals. The determined eutectic or first melting point (T_{FM}) of most 2-phase inclusions upon gentle heating, following their complete freezing falls within the range of -61 and -50 °C, while their last melting point of ice is about -10 to -0.4 °C. For 2-phase inclusions homogenizing to liquid phase with salinities above the 26.3 wt% $NaCl_{equiv}$, ice is melting first and hydrohalite is the last stable solid phase during the temperature increase following the complete freezing. The average hydrohalite melting point was obtained about -34 °C. Contrastingly, for 2-phase inclusions with salinities below 23.3 wt% $NaCl_{equiv}$, where ice is the last stable solid phase, the last melting point was measured about -20.5 to -21 °C.

The estimated salinity for 2-phase and multiphase inclusions range from 15 to 65 wt% $NaCl_{equiv}$ (Figure 8). Most of the values cluster between 25 to 45 wt% $NaCl_{equiv}$, mainly belonging to type 4 inclusions and testifying to a moderate to highly saline fluid. Two-phase inclusions have low salinities ranging from 17.77 to 28.66 wt% $NaCl_{equiv}$, with an average of 25.31 wt% $NaCl_{equiv}$. The lack of halite daughter mineral in this group is due to the fact that halite saturates at >26 wt% $NaCl_{equiv}$ at 25 °C and halite crystals are meta-stable at salinities between 20 and 30 wt% $NaCl_{equiv}$ (Shepherd et al., 1985; Bodnar and Vityk, 1994). Salinities above the 30 wt% $NaCl_{equiv}$ in Figure 8 belong to type 4 inclusions.

Additionally, the highest KCl content of those multiphase inclusions which had halite and sylvite solid crystals was estimated about 41 wt%, using the melting

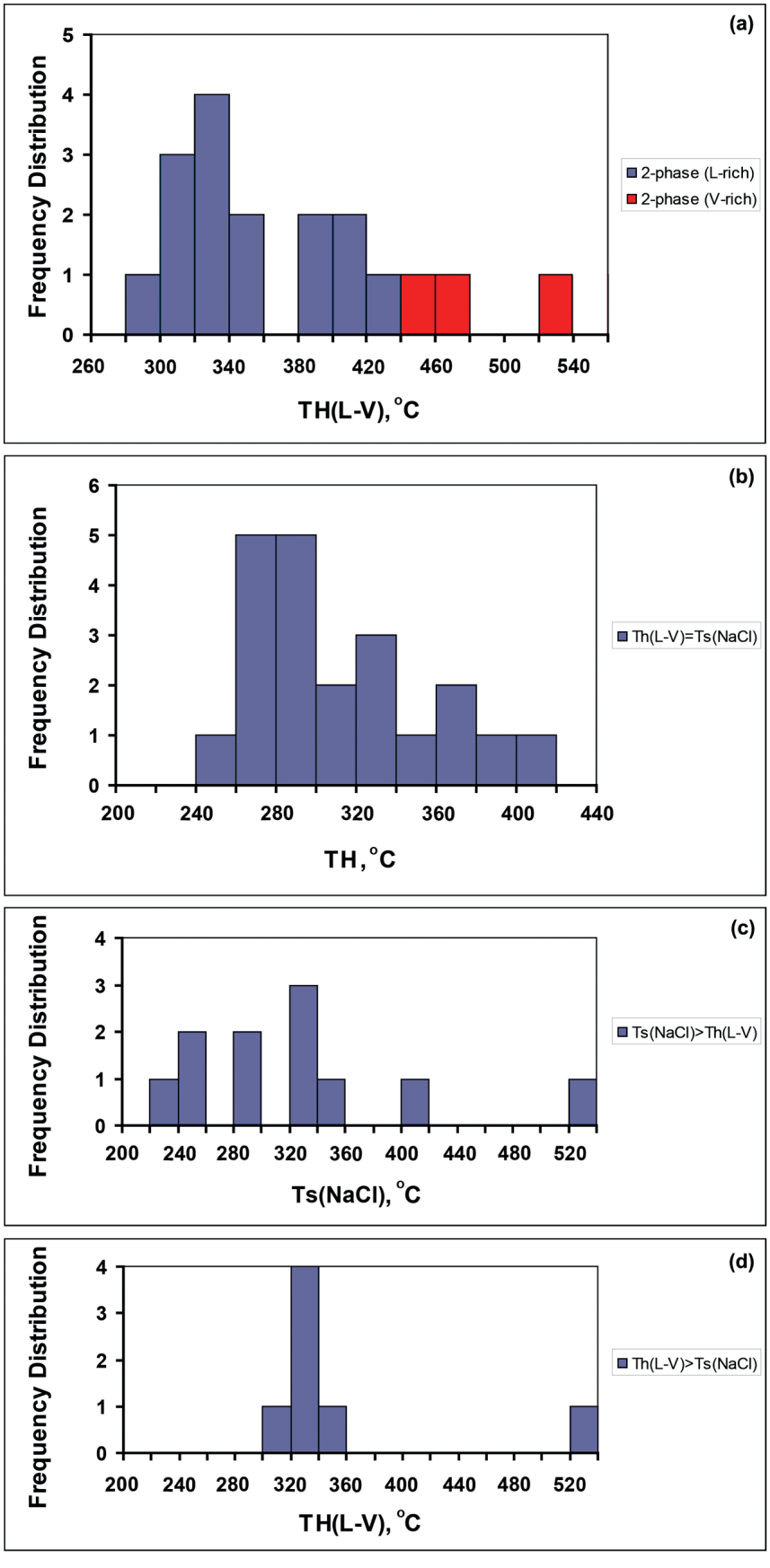

Figure 7. Frequency distribution histograms of homogenization temperatures measured on fluid inclusions within quartz-sulphide veinlets at Qarachilar. (a) 2-phase (type 2 and 3) fluid inclusions homogenizing to liquid phase and vapor phase, respectively; (b) multiphase (type 4) inclusions homogenizing by simultaneous dissolution of halite crystal and disappearance of vapor bubble; (c) type 4 inclusions homogenizing by dissolution of halite crystal; (d) type 4 inclusions homogenizing by disappearance of vapor bubble.

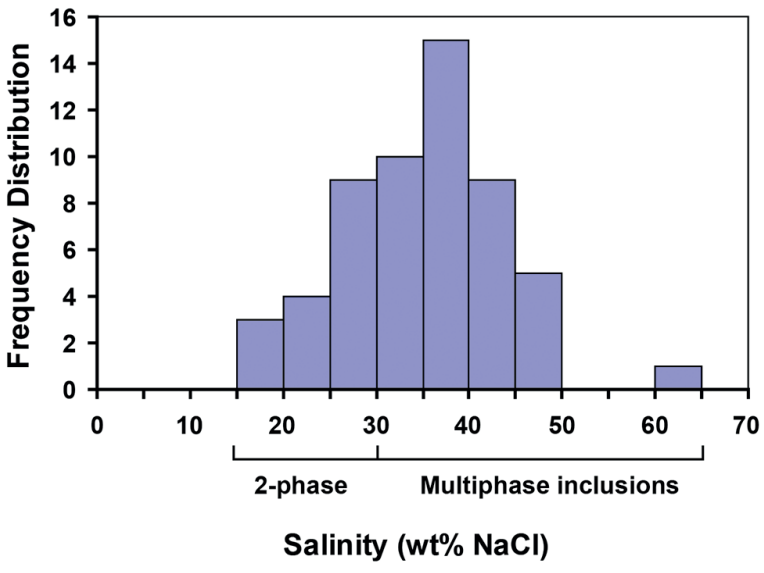

Figure 8. Frequency distribution histogram of salinities measured on 2-phase and multiphase fluid inclusions within quartz-sulphide veinlets at Qarachilar.

temperature of sylvite (165 °C; the highest measured $T_{m(sylvite)}$).

In this regard, two populations of inclusions are present: inclusions with low salinities (17.77 to 28.66 wt% $NaCl_{equiv}$) and without halite and sylvite daughter crystals and inclusions with moderate to high salinities containing halite and halite-sylvite daughter phases (Figure 8).

DISCUSSION

The measured eutectic temperatures measured (Te or TFM) on 2-phase fluid inclusions (about -61 to -50 °C) may indicate the presence of a poly-saline and multi-cation fluid containing Ca, Mg and Fe chlorides, in addition to NaCl and KCl (Borisenko, 1977; Chen et al., 2011; Deng et al., 2013a). The presence of $FeCl_2$ is also conceivable from observed opaque blebs within the fluid inclusions. Calcium and magnesium might have been supplied during the potassic alteration and by the destruction of Ca- and Mg-silicates (Ulrich et al., 2001; Rusk et al., 2004) or just the saline fluid was in equilibrium with Ca-Mg silicates. Furthermore, very negative eutectic temperatures may indicate the presence of unobservable amounts of CO_2, as the liquid CO_2 phase can only be observed in concentrations above 3 mole % (Ulrich et al., 2001).

None of the opaque daughter minerals were dissolved or decreased in size during the heating run. This can be resulted from post-entrapment hydrogen diffusion and the change in the redox state of the inclusions (Wilkinson, 2001), or may be due to their entrapment from ore-bearing fluid as suspended solid crystals.

Two distinct and separate populations of fluid inclusions are recognizable in salinity versus $T_{H(L-V)}$ plot (Figure 9). Type 4 inclusions are mainly plotted on or around the halite saturation curve, indicating entrapment from a NaCl-saturated fluid, while type 2 and 3 inclusions lie far below it, being entrapped from a NaCl-undersaturated fluid (Roedder, 1984). Type 4 inclusions plotted above the NaCl-saturation curve can be resulted in three ways: (1) entrapment from a NaCl-supersaturated fluid (2) necking down and/or loss of liquid (Audetat and Gunther, 1999), and (3) entrapment of solid halite crystals from hydrothermal fluids.

Based on this diagram, the vapor pressure of the NaCl-solution during the entrapment of 2-phase inclusions is estimated about 50 to 250 bars. Moreover, it can be conceived that hydrothermal fluid experienced saturation (with respect to NaCl) at temperatures about ≤392 °C.

The data points above the NaCl-saturation curve in Figure 9 show distributions along horizontal arrays, corresponding to the pressurization-depressurization and cooling trend. The wide range of salinity and T_H values obtained for the studied inclusions, similar to other porphyry and hydrothermal Cu-Mo deposits, may be resulted from the presence of various fluids with different physical and chemical characteristics at different times, as well as necking-down or leakage (Audetat and Gunther, 1999). Furthermore, data points in Figure 9 display an oblique trend towards the bottom left. In other words, with a decrease in the homogenization temperature, salinity is also decreased. This trend corresponds to the boiling of low-salinity hydrothermal fluids (e.g., Zhang et al., 2013; Deng et al., 2014), as well as dilution by superficial fluids (Figure 9; Shepherd et al., 1985). Therefore, it can be conceived that magmatic-hydrothermal aqueous ore-bearing fluids have experienced boiling and also mixing with low salinity-temperature superficial fluids.

According to Figure 9, it is revealed that ore-bearing fluids have started boiling at about 400 °C, following depressurization of the system. Subsequently a vapor phase has been separated from a saline aqueous liquid phase, manifested by inclusions, which have entrapped

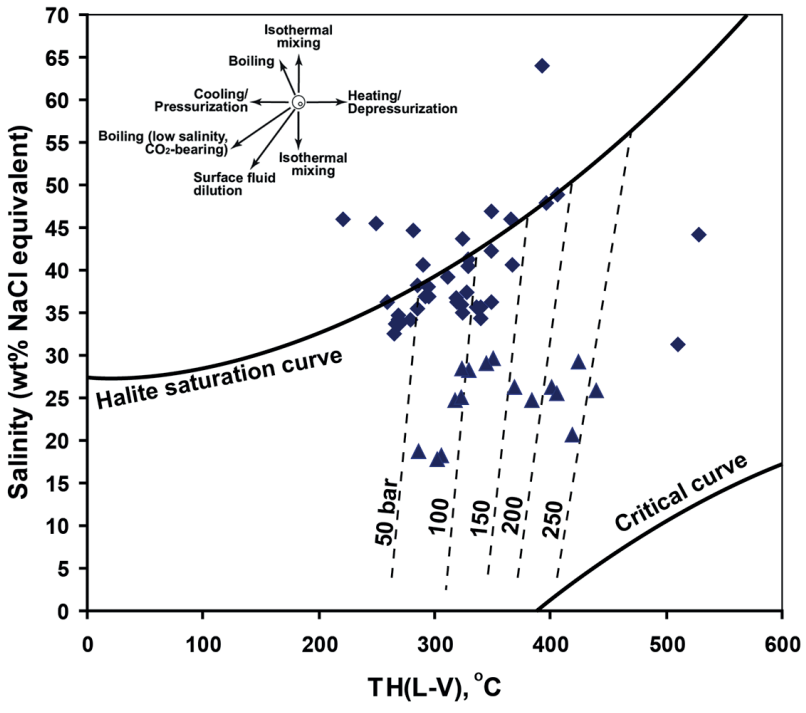

Figure 9. $T_{H(L-V)}$ vs. equivalent salinities (expressed as wt% $NaCl_{equiv}$) plot for measured fluid inclusions, illustrating the distribution pattern of the data points relative to the NaCl saturation and critical curves (NaCl saturation and critical curves from Ahmad and Rose, 1980; dashed lines referring to vapor pressures of NaCl solutions at the indicated temperatures and salinities from Roedder, 1984),

fluids with salinities about 48.9 wt% $NaCl_{equiv}$.

Another indication for occurrence of boiling is the presence of 2-phase and halite-bearing multiphase inclusions with rather similar homogenization temperatures (Figure 7). Meanwhile, the lack of multiphase vapor-rich inclusions with only opaque daughter crystals is contrary to the direct segregation of a saline fluid from the crystallizing magma (Wilkinson, 2001). Finally, the different phase ratios observed within inclusions of any type can also be attributed to the entrapment from a boiling and heterogeneous hydrothermal fluid (Wilkinson, 2001), though post-entrapment modifications of the fluid inclusions due to necking down or leakage must not be neglected.

Therefore, considering the occurrence of boiling for the studied fluid inclusions, especially those with $T_{m(NaCl)}$=/~$T_{H(L-V)}$, pressure correction of the obtained homogenization temperatures will be minor and negligible (Roedder and Bodnar, 1980; Wilkinson, 2001).

In $T_{m(NaCl)}$-$T_{H(L-V)}$ diagram (Figure 10), most of the data points are plotted around the diagonal line. The vertical arrays above the diagonal line may indicate the entrapment of solid halite crystals from the heterogeneous boiling fluid. Inclusions homogenizing by halite dissolution have entrapped at the low-temperature part of the liquid stability field, where no coexisting vapor phase is present, whereas inclusions homogenizing by vapor disappearance indicate fluid entrapment at high-temperature part of the liquid stability field in the presence of vapor phase (Roedder and Bodnar, 1980; Bodnar, 1994; Cline and Bodnar, 1994; Zhang et al., 2007).

The discrepancy between $T_{m(NaCl)}$ and $T_{H(L-V)}$ may reflect the relative pressure of the system. For inclusions plotted around or on the diagonal line, this value ranges from 4 to 30 °C, with an average of 16 °C. Such inclusions with low discrepancies ($T_{m(NaCl)}$ ~ $T_{H(L-V)}$) can be attributed to entrapment from a heterogeneous boiling

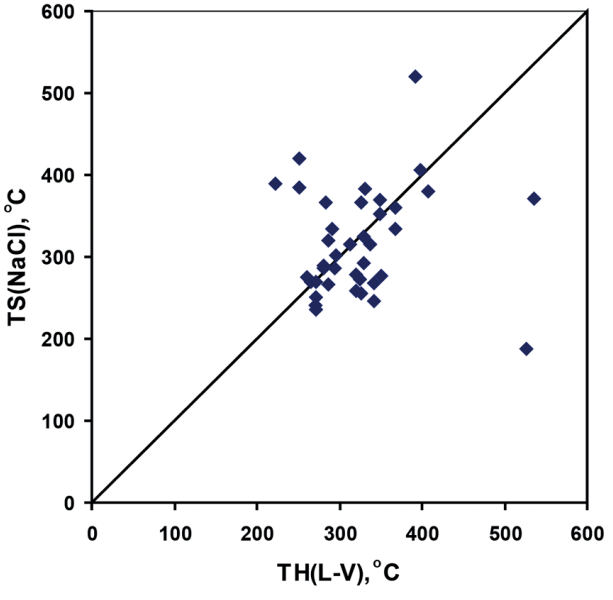

Figure 10. Liquid-vapor homogenization temperature [$T_{H(L-V)}$] vs. halite dissolution temperature [$T_{m(NaCl)}$] for halite-bearing inclusions at Qarachilar (the diagonal line corresponds to $T_{H(L-V)}/T_{m(NaCl)}$=1; Shepherd et al., 1985).

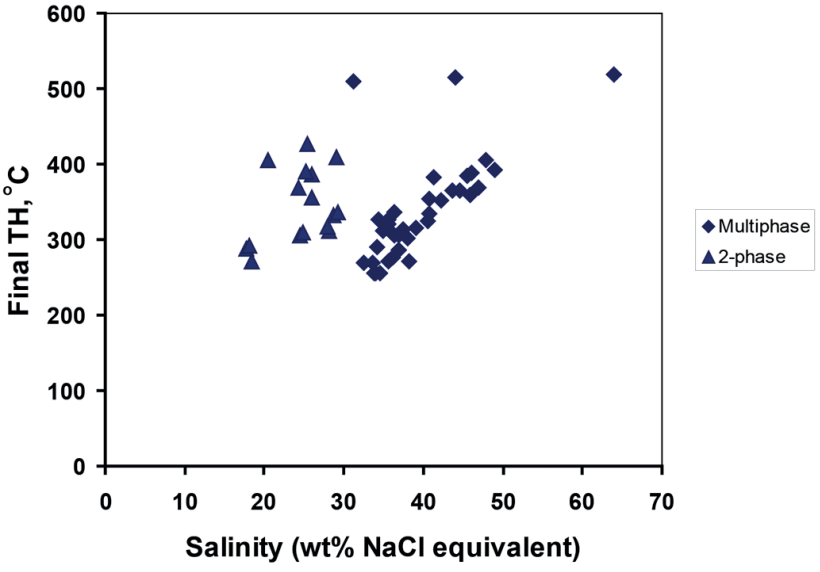

Figure 11. $T_{H(Final)}$ vs. equivalent salinity (expressed as wt% $NaCl_{equiv}$) plot, showing the positive linear correlation and linear trend for type 4 inclusions.

fluid (Shepherd et al., 1985). However, there is another group of multiphase inclusions, which plot far above or below the diagonal line, for which the discrepancy between $T_{m(NaCl)}$ and $T_{H(L-V)}$ ranges between 34 and 320 °C, with an average of 100 °C. High discrepancies may refer to fluid entrapment at high-pressure condition, which may be present just before the occurrence of hydro-fracturing (Cline and Bodnar, 1994). On the other hand, necking-down (Ahmad and Rose, 1980; Audetat and Gunther, 1999) and/or solid phase entrapment may also lead to such high discrepancies.

In $T_{H(Final)}$ vs. salinity plot (Figure 11), halite-bearing multiphase (type 4) inclusions show positive correlation between these two parameters and a linear trend with almost constant slope, which is also reported from many other porphyry deposits (Cloke and Kessler, 1979; Roedder, 1984).

The estimated bulk density for type 2 and 3 inclusions is between 0.8 and 1.0 g/cm^3, while it is about 1.0-1.2 g/cm^3 for high-salinity type 4 inclusions (Zhang and Frantz, 1987; Figure 12). Furthermore, a negative correlation is present between the density and $T_{H(L-V)}$ values of multiphase inclusions, indicating that the density of entrapped fluids increases with decreasing of homogenization temperature and increasing of the salinity. Such a wide range of estimated bulk density values in a coexisting set of inclusions testifies to entrapment from heterogeneous, supersaturated and boiling fluids during boiling events (Wilkinson, 2001).

Based on the density of NaCl solution versus homogenization temperature diagram (Shepherd et al., 1985), the minimum estimated pressures for the studied 2-phase inclusions with $T_{H(L-V)}$ values about 285-440 °C (a mean of 357 °C) and salinities about 17.77 to 28.66 wt%

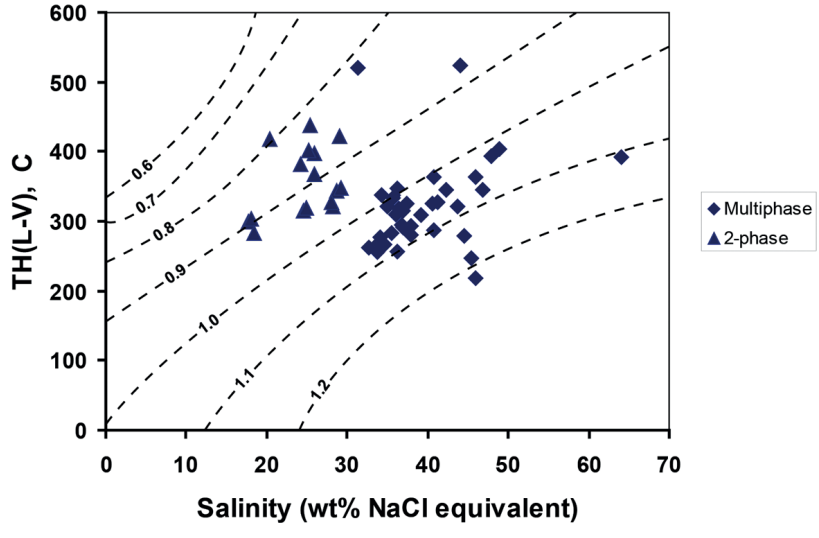

Figure 12. $T_{H(L-V)}$ vs. equivalent salinities (expressed as wt% $NaCl_{equiv}$) plot showing densities (g/cm^3) of the studied NaCl-H_2O fluid inclusions (Wilkinson 2001). Contours regressed from data generated by the equation-of-state of Zhang and Frantz (1987).

$NaCl_{equiv}$ (an average of 25.31 wt% $NaCl_{equiv}$) ranges from 50 to 300 bars, though most of the measured inclusions show pressures about 50 to 120 bar, which is equal to the hydrostatic depths of 470-1100m. Additionally, the estimated boiling depth for 2-phase inclusions based on Hass (1971) yielded depths of 800 to 1000 m.

Based on the pressure-T_H diagram for multiphase fluid inclusions (Roedder and Bodnar, 1980), the estimated minimum pressure during the entrapment of type 4 inclusions with $T_{m(NaCl)}$=/~$T_{H(L-V)}$ is about 50-200 bars, but mainly ranging between 50 and 100 bars, which is equivalent to the hydrostatic pressure heads of about 470-950 m. Furthermore, the boiling depths calculated for those with estimated pressures of 160-170 bars and 190-200 bars are about 1500 and 1900m, respectively.

However, type 4 inclusions with $T_{m(NaCl)}$>$T_{H(L-V)}$ show 2 ranges of pressure. For the inclusions with discrepancies below 100°C, the yielded pressure mainly ranges between 50 and 100 bar, with few data around 120 and 150 bar, but for those with discrepancies above the 100 °C, values as high as 730 and 1400 bar are also obtained, which are equal to the hydrostatic depths of about 3300 and 5640 m, respectively. Such exceptionally high estimated values, especially for the second group of type 4 inclusions cannot be realistic, as two adjacent inclusions in a single quartz crystal can not entrap two different fluids at such enormously different pressures. Solid halite entrapment from a heterogeneous fluid will lead to the shifting of $T_{m(NaCl)}$ to much higher values in a similar $T_{H(L-V)}$. In such a case, the variation of salinity values for such inclusions may depend mainly on the size of the trapped solid halite crystal and thus, their salinity and final homogenization temperature will be abnormally higher than other coexisting inclusions and definitely does not represent the real salinity of hydrothermal fluids. Furthermore, these inclusions may have been entrapped once the system was suffered trans-compression under predominant lithostatic condition. Necking-down and/or loss of liquid can also produce fluid inclusions with large $T_{H(L-V)}$ and $T_{m(NaCl)}$ discrepancies (Ahmad and Rose, 1980; Audetat and Gunther, 1999). Based on these considerations, the approximately estimated depth of the mineralization, regardless of the likely false pressures mentioned above, ranges from 500 to 1100 m below the paleo-topographic surface.

Very few observations of CO_2-bearing inclusions within the studied samples also indicate that phase immiscibility has occurred at shallow depths, as the CO_2 content of magma is higher at much deeper settings and its solubility in felsic magmas declines while the pressure and/or temperature decreases (Lowenstern, 2001; Wilkinson, 2001).

At the end, it must be mentioned that the microthermometry results of the quartz-sulphide veins-veinlets in Qarachilar area show striking resemblance with other neighboring PCDs in the area, such as Sungun PCD (Hezarkhani and William-Jones, 1998; Calagari, 2004b) and Kighal porphyry copper prospect (Simmonds, 2010; Simmonds et al., 2015), located 30 and 40 km southeast of it, respectively. Furthermore, T_H and salinity values obtained in this study correlate well with the ranges proposed for porphyry deposits by Wilkinson (2001) (250-800 °C and 10-90 wt% $NaCl_{equiv}$). Such wide ranges of salinities and homogenization temperatures for 2-phase and multiphase inclusions are also reported by many workers from typical porphyry copper deposits throughout the world (e.g. Etminan, 1978; Wilkinson, 2001; Gonzalez-Partida and Levresse, 2003; Landtwing et al., 2010; Li et al., 2012; Deng et al., 2013b; Wu et al., 2014).

CONCLUSIONS

Mineralization in the central part of the Qaradagh pluton has occurred as quartz-sulphide and mono-mineralic sulphide veins and veinlets, containing pyrite, chalcopyrite and molybdenite as the main ore minerals. These veins and veinlets have variable thicknesses, ranging between several mm to <1 m, illustrating compact, massive, brecciated and honeycomb textures and re-opening evidence. The fluid inclusions entrapped within the quartz grains of these veins and veinlets are of monophase vapor, 2-phase (liquid-vapor) and multiphase (containing halite and sometimes sylvite and opaque daughter crystals) types. Microthermometric studies performed on the 2-phase and multiphase inclusions within these veins showed that the salinity of entrapped fluids ranges from 15 to 65 wt% $NaCl_{equiv}$, with the highest frequency between 25 and 45 wt% $NaCl_{equiv}$. The 2-phase inclusions have lower salinities below 30 wt% $NaCl_{equiv}$, while the multiphase inclusions are characterized by salinities above the 30 wt% $NaCl_{equiv}$.

The homogenization temperature obtained for the primary 2-phase and multiphase inclusions ranges between 220 and 540 °C. Most of the 2-phase inclusions homogenize by vapor disappearance (type 2) with the $T_{H(L-V)}$ values between 280 and 440 °C and the highest frequency between 300 and 360 °C. A few of the 2-phase inclusions homogenize into vapor state (type 3) for which, higher $T_{H(L-V)}$ values between 440 and 540 °C are obtained. Type 4 inclusions show 3 modes of homogenization. Most of them homogenize by simultaneous disappearance of vapor bubble and dissolution of halite daughter crystal for which, the T_H value is about 240-420 °C (mostly between 260 and 340 °C). Some of them are homogenized by halite dissolution with $T_{m(NaCl)}$ values about 220-360 °C. Finally, a few multiphase inclusions homogenize by vapor disappearance, which have $T_{H(L-V)}$ values between 300 and 360 °C.

The data-points trend in the $T_{H(L-V)}$-Salinity plot

testifies to the occurrence of boiling of low-salinity fluids and dilution by superficial fluids. Therefore, it can be concluded that the ore-forming magmatic-hydrothermal aqueous fluids have most likely experienced boiling phenomena and also mixed with low temperature and low salinity superficial fluids. Other evidence supporting the occurrence of boiling includes coexistence of liquid-rich and vapor-rich 2-phase inclusions, as well as multiphase halite-bearing inclusions, which homogenize in a similar range of T_H. Therefore, the main process that led to the precipitation of ore minerals in the studied veins-veinlets was found to be liquid-vapor immiscibility (boiling) and consequent super-saturation of the hydrothermal fluids in a restricted rock volume. Meanwhile, the minimum pressure at the time of entrapment for the fluid inclusions was calculated about 50 to 120 bars, which is equal to the hydrostatic depth of 500-1100 m below the paleo-surface.

The measured homogenization temperatures and salinities are in the range proposed for porphyry copper deposits and show common ranges with the adjacent Sungun and Kighal porphyry copper deposit and prospect, though the genesis of mineralization in the area is controversial, including suggestions of intrusion-related gold (Mokhtari, 2008; Mokhtari et al., 2013), vein-type Cu-Mo-Au (Rezai Aghdam and Sohrabi, 2010), as well as porphyry type Cu-Mo mineralization (e.g., Amini Fazl, 1994; Zakeri et al., 2011; Zakeri, 2013).

ACKNOWLEDGEMENTS

Authors would like to express their appreciation to the Deputy Dean of the Research Bureau of Tabriz University (Tabriz-IRAN), which financially supported this study through the grant No. 27/338/8. Thanks are also extended to the anonymous reviewers and the editor of the journal for their constructive comments, which helped to improve the manuscript significantly. Authors also thank Dr. Leila Zakeri for her collaboration in sampling stage.

REFERENCES

Ahmad S.N. and Rose A.W. (1980) Fluid inclusions in porphyry and skarn ore at Santa Rita, New Mexico. Economic Geology 75, 229-250.

Alavi M. (1991) Sedimentary and structural characteristics of the paleo-Tethys remnants in northeastern Iran. Geological Society of America Bulletin 103, 983-992.

Amini Fazl A. (1994) Petrology, mineralogy and geochemistry of Qaradagh intrusive body (Ordubad granite) at NW Iran (Ghoolan, Doozal, Astamal). Ph.D. thesis, Azerbaijan Republic Academy of Sciences, Baku, Azerbaijan, 258 pp.

Audétat A. and Günther D. (1999) Mobilization and H_2O-loss from fluid inclusions in natural quartz crystals. Contributions to Mineralogy and Petrology 137, 1-14.

Berberian M. and King G.C.P. (1981) Towards a paleogeography and tectonic evolution of Iran. Canadian Journal of Earth Sciences 18, 210-265.

Bodnar R.J. (1993) Revised equation and table for determining the freezing point depression of H_2O-NaCl solutions. Geochimica et Cosmochimica Acta 57, 683-684.

Bodnar R.J. (1994) Synthetic fluid inclusions: XII. The system H_2O-NaCl. Experimental determination of the halite liquidus and isochors for a 40 wt% NaCl solution. Geochimica et Cosmochimica Acta 58, 1053-1063.

Bodnar R.J. (2003) Introduction to fluid inclusions. In: Fluid inclusion-analysis and interpretation. (eds): I. Samson, A. Anderson, D. Marshall, Mineralogical Association of Canada, Short Course Series 32, 1-9.

Bodnar R.J. and Vityk M.O. (1994) Interpretation of microthermometric data for H_2O-NaCl fluid inclusions. In: Fluid inclusions in minerals, methods and applications. (eds): B. De Vivi and M.L. Frezzoti, Blacksburg, Virginia Polytechnic Institute, 117-130.

Borisenko A.S. (1977) Study of the salt composition of solutions in gas-liquid inclusions in minerals by cryometric method. Soviet Geology and Geophysics 18, 11-19.

Bouzari F. and Clark A.H. (2006) Prograde evolution and geothermal affinities of a major porphyry copper deposit: The Cerro Colorado hypogene protore, I Region, northern Chile. Economic Geology 101, 95-134.

Calagari A.A. (1997) Geochemical, stable isotope, noble gas and fluid inclusion studies of mineralization and alteration at Sungun porphyry copper deposit, East-Azarbaidjan, Iran: Implication for genesis. Ph.D. thesis, University of Manchester, 537pp.

Calagari A.A. (2004a) Geology and fracture-related hypogene hydrothermal alteration and mineralization of porphyry copper deposit at Sungun, Iran. Journal of Geological Society of India 64, 595-618.

Calagari A.A. (2004b) Fluid inclusion studies in quartz veinlets in the porphyry copper deposit at Sungun, East-Azarbaidjan, Iran. Journal of Asian Earth Sciences 23, 179-189.

Chen H., Kyser T.K., Clark A.H. (2011) Contrasting fluids and reservoirs in the contiguous Marcona and Mina Justa iron oxide-Cu (-Ag-Au) deposits, south-central Peru. Mineralium Deposita 46, 677-706.

Cline J.S. and Bodnar R.J. (1994) Direct evolution of brine from a crystallizing silicic melt at the Questa, New Mexico, molybdenum deposit. Economic Geology 89, 1780-1802.

Cloke P.L. and Kesler S.E. (1979) The halite trend in hydrothermal solutions. Economic Geology 74, 1823-1831.

Deng X.H., Chen Y.J., Santosh M., Yao J.M. (2013a) Genesis of the 1.76 Ga Zhaiwa Mo-Cu and its link with the Xiong'er volcanics in the North China Craton: Implications for accretionary growth along the margin of the Columbia supercontinent. Precambrian Research 227, 337-348.

Deng X.H., Chen Y.J., Santosh M., Yao J.M. (2013b) Re-Os geochronology, fluid inclusions and genesis of the 0.85 Ga Tumen molybdenite-fluorite deposit in Eastern Qinling, China: Implications for pre-Mesozoic Mo-enrichment and tectonic setting. Geological Journal 48, 484-497.

Deng X.H., Santosh M., Yao J.M., Chen Y.J. (2014) Geology, fluid inclusions and sulphur isotopes of the Zhifang Mo deposit in Qinling Orogen, central China: a case study of orogenic-type Mo deposits. Geological Journal 49, 515-533.

Etminan H. (1978) Fluid inclusion studies of the porphyry copper ore bodies at Sar-Cheshmeh, Darreh Zar and Mieduk (Kerman region, southeastern Iran) and porphyry copper

discoveries at Miduk, Gozan, and Kighal, Azarbaijan region (northwestern Iran). International Association on the Genesis of Ore Deposits, 5th Symposium, Snowbird, Utah, Proceedings, 88 pp.

Goldstein R.H. (2003) Petrographic analysis of fluid inclusions. In: Fluid inclusion-analysis and interpretation. (eds): I. Samson, A. Anderson, D. Marshall Mineralogical Association of Canada, Short Course Series 32, 9-54.

Gonzalez-Partida E. and Levresse G. (2003) Fluid inclusion evolution at the La Verde porphyry copper deposit, Michocan, Mexico. Journal of Geochemical Exploration 78-79, 623-626.

Hass J.L. (1971) The effect of salinity on the maximum thermal gradient of a hydrothermal system at hydrostatic pressure. Economic Geology 66, 940-946.

Hedenquist J.W., Arribas A.J., Reynolds T.J. (1998) Evolution of an intrusion-centered hydrothermal system: Far Southeast-Lepanto porphyry and epithermal Cu-Au deposits, Philippines. Economic Geology 93, 373-404.

Hezarkhani A. and William-Jones A.E. (1998) Controls of alteration and mineralization in the Sungun porphyry copper deposit, Iran: Evidence from fluid inclusions and stable Isotopes. Economic Geology 93, 651-670.

Kranz R.L. (1983) Micro-cracks in rocks: A review. Tectonophysics 100, 449-480.

Landtwing M.R., Furrer C., Redmond P.B., Pettke T., Guillong M., Heinrich C.A., (2010) The Bingham Canyon porphyry Cu-Mo-Au deposit: III. Zoned copper-gold ore deposition by magmatic vapor expansion. Economic Geology 105, 91-118.

Li N., Ulrich T., Chen Y.J., Thomsen T.B., Pease V., Pirajno F. (2012) Fluid evolution of the Yuchiling porphyry Mo deposit, East Qinling, China. Ore Geology Reviews 48, 442-459.

Lowenstern J.B. (2001) Carbon dioxide in magmas and implications for hydrothermal systems. Mineralium Deposita 36, 490-502.

Mehrpartou M., Mirzaei M., Alaei S. (1997) Geologic map of Siahrood. Geological Survey of Iran, Tehran, scale 1:100 000, 1 sheet.

Mokhtari M.A.A. (2008) Petrology, geochemistry and petrogenesis of Qaradagh batholith (east of Siahrood, East Azarbaidjan) and its related skarn. Ph.D. thesis, University of Tarbiat Modarres, Tehran, 290 pp.

Mokhtari M.A.A., Moein Vaziri H., Ghorbani M.R., Mehrparto M. (2005) Petrography and petrology of Ghoolan batholith (north of Azarbaidjan). 24th Earth Sciences Congress, Tehran, Geological Society of Iran.

Mokhtari M.A.A., Moein Vaziri H., Ghorbani M.R., Mehrparto M. (2013) Geology and geochemistry of Aniq-Qarachilar Au-Cu-Mo mineralization (NE of Kharvana, eastern Azarbaijan). Geosciences 90, 135-150 (in Persian).

Rezai Aghdam M. and Sohrabi G. (2010) Investigation on the geochemistry of alteration and its relationship with the Mo and Cu mineralization in Gharachilar-Gharadareh area (NW Iran). Journal of Science of Islamic Azad University 77, 129-149.

Roedder E. (1984) Fluid Inclusions. Mineralogical Society of America, Review in Mineralogy 12, 644 pp.

Roedder E. and Bodnar R.J. (1980) Geologic pressure determinations from fluid inclusion studies. Annual Review of Earth and Planetary Sciences 8, 261-301.

Rusk B.G., Reed M.H., Dilles J.H., Klemm L.M., Heinrich C.A. (2004) Compositions of magmatic hydrothermal fluids determined by LA-ICP-MS of fluid inclusions from the porphyry copper-molybdenum deposit at Butte, MT. Chemical Geology 210, 173-199.

Seedorff E. and Einaudi M. (2004) Henderson porphyry molybdenum system, Colorado: II. Decoupling of introduction and deposition of metals during geochemical evolution of hydrothermal fluids. Economic Geology 99, 39-72.

Shahabpour J. (1982) Aspects of alteration and mineralization at the Sar-Cheshmeh copper-molybdenum deposit, Kerman, Iran. Ph.D. thesis, University of Leeds, 342 pp.

Shepherd T.J., Rankin A.H., Alderton D.H.M. (1985) A practical guide to fluid inclusion studies. Blackie, Glasgow, 239 pp.

Simmonds V. (2010) Studies of geology, geochemistry and genesis of porphyry-type copper mineralization in Kighal and Barmolk areas, north of Varzeghan, East-Azarbaidjan, Iran. Ph.D. thesis, University of Tabriz, 195 pp.

Simmonds V., Calagari A.A., Kyser K. (2015) Fluid inclusion and stable isotope studies of the Kighal porphyry Cu-Mo prospect, East-Azarbaidjan, NW Iran. Arabian Journal of Geosciences 8, 437-453.

Simmonds V. and Moazzen M. (2015) Re-Os dating of molybdenites from Oligocene Cu-Mo-Au mineralized veins in the Qarachilar area, Qaradagh batholith (northwest Iran): implications for understanding Cenozoic mineralization in South Armenia, Nakhchivan and Iran. International Geology Review 57, 290-301.

Sterner S.M., Hall D.L., Bodnar R.J. (1988) Synthetic fluid inclusions: V. Solubility relations in the system NaCl-KCl-H_2O under vapor-saturated conditions. Geochimica et Cosmochimica Acta 52, 989-1005.

Ulrich T., Guenther D., Heinrich C.A. (2001) The evolution of a porphyry Cu-Au deposit, based on LA-ICP-MS analysis of fluid inclusions; Bajo de la Alumbrera, Argentina. Economic Geology 96, 1743-1774.

Vollbrecht A. (1989) Microriβ-Analyse im KTB-Datenerhebung U-Tisch Mikroskopie. Unpublished report IGDL, Gottingen.

Wanhainen C., Broman C., Martinsson O. (2003) The Aitik Cu-Au-Ag deposit in northern Sweden: A product of high salinity fluids. Mineralium Deposita 38, 715-726.

Whitney D.L. and Evans B.W. (2010) Abbreviations for names of rock-forming minerals. American Mineralogist 95, 185-187.

Wilkinson J.J. (2001) Fluid inclusions in hydrothermal ore deposits. Lithos 55, 229-272.

Wu Y.S., Wang P., Yang Y.F., Xiang N., Li N., Zhou K.F. (2014) Ore geology and fluid inclusion study of the Donggebi giant porphyry Mo deposit, Eastern Tianshan, NW China. Geological Journal 49, 559-573.

Zakeri L. (2013) Investigation on geology, mineralization, alteration, geochemistry and genesis of Gharachilar ore deposit, Shah Jahan batholith (East Azarbaidjan). Ph.D. thesis, University of Tabriz, 282 pp.

Zakeri L., Malek-Ghasemi F., Jahangiri A., Moazzen M. (2011) Metallogenic implications of biotite chemical composition: Sample from Cu-Mo-Au mineralized granitoids of the Shah Jahan Batholith, NW Iran. Central European Geology 54, 271-294.

Zhang Y.G. and Frantz J.D. (1987) Determination of the homogenization temperatures and densities of supercritical

fluids in the system NaCl-KCl-$CaCl_2$-H_2O using synthetic fluid inclusions. Chemical Geology 64, 335- 350.

Zhang D., Xu G., Zhang W., Golding S.D. (2007) High salinity fluid inclusions in the Yinshan polymetallic deposit from the Le-De metallogenic belt in Jiangxi Province, China: Their origin and implications for ore genesis. Ore Geology Review 31, 247-260.

Zhang L., Zheng Y., Chen Y.J. (2012) Ore geology and fluid inclusion geochemistry of the Tiemurt Pb-Zn-Cu deposit, Altay, Xinjiang, China: A case study of orogenic-type Pb-Zn systems. Journal of Asian Earth Sciences 49, 69-79.